Biomaterials 34 (2013) 9190–9200

Contents lists available at ScienceDirect

Biomaterials

journal homepage: www.elsevier.com/locate/biomaterials

Multifunctional receptor-targeted nanocomplexes for the delivery of therapeutic nucleic acids to the Brain☆

Gavin D. Kenny[a,b], Alison S. Bienemann[c], Aristides D. Tagalakis[a], John A. Pugh[d], Katharina Welser[e], Frederick Campbell[e], Alethea B. Tabor[e], Helen C. Hailes[e], Steven S. Gill[c], Mark F. Lythgoe[b], Cameron W. McLeod[d], Edward A. White[c], Stephen L. Hart[a,*]

[a] Molecular Immunology Unit, UCL Institute of Child Health, London WC1N 1EH, UK
[b] Centre for Advanced Biomedical Imaging, Department of Medicine and Institute of Child Health, University College London, London WC1E 6DD, UK
[c] Functional Neurosurgery Research Group, School of Clinical Sciences, AMBI Labs, University of Bristol, Southmead Hospital, Bristol BS10 5NB, UK
[d] Centre For Analytical Sciences, University of Sheffield, Sheffield S10 2TN, UK
[e] Department of Chemistry, University College London, London WC1H 0AJ, UK

ARTICLE INFO

Article history:
Received 4 July 2013
Accepted 23 July 2013
Available online 12 August 2013

Keywords:
Gene therapy
Magnetic resonance imaging (MRI)
Nanoparticles
Convection enhanced delivery (CED)
Peptide

ABSTRACT

Convection enhanced delivery (CED) is a method of direct injection to the brain that can achieve widespread dispersal of therapeutics, including gene therapies, from a single dose. Non-viral, nanocomplexes are of interest as vectors for gene therapy in the brain, but it is essential that administration should achieve maximal dispersal to minimise the number of injections required. We hypothesised that anionic nanocomplexes administered by CED should disperse more widely in rat brains than cationics of similar size, which bind electrostatically to cell-surface anionic moieties such as proteoglycans, limiting their spread. Anionic, receptor-targeted nanocomplexes (RTN) containing a neurotensin-targeting peptide were prepared with plasmid DNA and compared with cationic RTNs for dispersal and transfection efficiency. Both RTNs were labelled with gadolinium for localisation in the brain by MRI and in brain sections by LA-ICP-MS, as well as with rhodamine fluorophore for detection by fluorescence microscopy. MRI distribution studies confirmed that the anionic RTNs dispersed more widely than cationic RTNs, particularly in the corpus callosum. Gene expression levels from anionic formulations were similar to those of cationic RTNs. Thus, anionic RTN formulations can achieve both widespread dispersal and effective gene expression in brains after administration of a single dose by CED.

1. Introduction

Genetic therapies involve the enhancement, replacement, modification, regulation and silencing of gene expression and offer great promise for the treatment of a wide range of diseases, of the central nervous system (CNS), including neurodegenerative, neuromuscular and metabolic diseases as well as cancers, many of which are currently untreatable [1–5]. Safe, but efficient delivery of therapeutic nucleic acids, however, remains a major technological barrier to the development of clinical therapeutics of the CNS. Nanocomplexes for gene delivery are of interest as alternatives to viral vectors as they can package a wider range of nucleic acids ranging from siRNA molecules of 20 or so nucleotides to tens of kilobases of plasmid DNA, and are less immunogenic than viruses allowing more effective repeated dosing of gene therapies [6,7]. Nanocomplexes may be delivered to the brain by the systemic route or by direct injection. Systemic delivery is limited in efficacy by the almost impermeable nature of the blood brain barrier (BBB) and rapid clearance of nanocomplexes from the circulation by the reticuloendothelial system (RES), particularly in the liver [8–10]. Direct injection methods such as intraparenchymal, intracerebroventricular and intrathecal injection, depend on diffusion for drug dispersal and so are limited in their dispersal by drug concentration and require injections at multiple sites to achieve widespread coverage of the brain.

In recent years, convection-enhanced delivery (CED) has been shown to achieve widespread distribution of therapeutics in the

* Corresponding author.
E-mail address: s.hart@ucl.ac.uk (S.L. Hart).

0142-9612/$ – see front matter © 2013 The Authors. Published by Elsevier Ltd. All rights reserved.
http://dx.doi.org/10.1016/j.biomaterials.2013.07.081

brain from a single administration [11], including viral gene therapy vectors [12–14]. CED utilises extremely fine intracranial catheters, implanted directly into the brain or spinal cord and distributes therapeutic agents along a pressure gradient generated between the catheter tip and the extracellular space, achieving controlled, homogeneous distribution of drugs over distances of up to 5 cm from the catheter tip in human brains [15]. Clinical trials involving administration of nanoparticles for gene therapy into the brain by CED have already been performed in patients with primary brain tumours [16,17], but more efficient formulations are required that achieve widespread dispersal and therapeutic delivery from a single administration.

Previous studies have shown that for widespread dispersal in the brain by CED, nanoparticles should be anionic or neutral rather than positively charged [18–20] and less than 200 nm [20]. Anionic liposomal complexes, however, have not been developed as extensively as cationic gene delivery complexes due to poor packaging of DNA and poor transfection efficiency [21,22]. In recent studies nucleic acid packaging into anionic complexes has been improved by various strategies, one of which involved combining anionic liposomes with polycationic protamine as an electrostatic bridge between the liposome and the nucleic acid [23,24]. In this study we have used a similar strategy to formulate an anionic receptor-targeted nanocomplex (RTN) comprising a mixture of a peptide containing a cationic oligolysine domain for DNA packaging and a neurotensin, receptor-targeting domain, and an anionic liposome. A similar cationic RTN formulation described previously [25] was also prepared containing the same peptide and plasmid, but a cationic liposome instead of an anionic liposome. In this study anionic and cationic RTNs, labelled with a gadolinium contrast agent and a rhodamine fluorophore, were compared for their biophysical properties then administered to rat brains by CED and their distribution analysed by MRI in whole brain and in tissue sections by LA-ICP-MS and fluorescence microscopy. Transgene expression was assessed by qRT-PCR and fluorescence microscopy for green fluorescent protein (GFP) reporter gene expression.

2. Materials and methods

2.1. Materials

Lipids (Supplementary Table 1); 1,2-dioleoyl-sn-glycero-3-phospho-(1′-rac-glycerol) (DOPG), 1,2-dioleoyl-3-trimethylammonium-propane (DOTAP), 1,2-dioleoyl-*sn*-glycero-3-phosphoethanolamine-N-(lissamine rhodamine B sulfonyl) (DOPE-Rhodamine) and 1,2-dioleoyl-sn-glycero-3-phosphoethanolamine (DOPE) were purchased from Avanti Polar Lipids Inc. (Alabaster, Alabama, USA). GdDOTA(-$GAC_{12})_2$ was synthesised as described by Kielar et al. [26]. Neurotensin (Nt) targeting peptide, its scrambled version (NtS) and the control peptide K_{16} (Supplementary Table 2) were synthesized on a MultiSynTech Syro peptide synthesizer using commercially available Fmoc amino acids (Novabiochem, Nottingham, UK) and standard automated protocols, as described previously [25]. The plasmid pCI-Luc consists of the luciferase gene from pGL3 (Invitrogen, Paisley, UK) subcloned into pCI (Promega, Southampton, UK). The plasmid pEGFP-N1 (4.7 kb) containing the gene for enhanced green fluorescent protein (GFP) was obtained from Clontech (Basingstoke, UK). 100 nm polystyrene nanospheres were purchased from Phosphorex Inc. (Hopkinton, MA, USA) with both cationic (+48.1 mV, orange Ex/EM 520/540 nm) and anionic (−47.9 mV, blue Ex/Em 360/440 nm) charges. The oligonucleotide primers and standards for qRT-PCR were provided by qStandard (Middlesex, UK) and were as follows: eGFP: forward primer 5′-CTTCAAGATCCGC CACAACAT-3′ and reverse primer 5′-GGTGCTCAGGTAGTGGTTGTC-3′; Rpl13: forward primer 5′-CCCTACAGTTAGATACCACACCAA-3′ and reverse primer 5′-GATAC-CAGCCACCCTGAGC-3′; Beta actin: forward primer 5′- ACGGTCAGGTCATCACTATCG-3′ and reverse primer 5′-AGCCACCAATCCACACAGA-3′; Sdha: forward primer 5′-TGGACCTTGTCGTCTTTGG-3′ and reverse primer 5′-TTTGCCTTAATCGGAGGAAC-3′.

2.2. Liposome formulation

Liposomes were formulated with lipid mixtures at specific molar ratios as follows; cationic liposomes DOTAP:DOPE:DOPE-Rhodamine:GdDOTA$(GAC_{12})_2$ and anionic liposomes DOPG:DOPE:DOPE-Rhodamine:GdDOTA$(GAC_{12})_2$ both at a molar ratio of 35:49:1:15 mol% respectively. Liposomes were prepared by dissolving the individual lipids in chloroform at 10 mg/mL and mixing them together, followed by rotary evaporation to produce a thin lipid film. Lipids were then rehydrated with sterile water whilst rotating overnight and then sonicated for an hour in a water bath to reduce the size to unilamellar liposomes.

2.3. Nanocomplex formulation and biophysical characterisation

LPD nanocomplex formulations were prepared by mixing aqueous solutions of anionic liposome (L), peptide (P) and plasmid DNA (D) at charge ratios of 3:2:1 (14.1:1.15:1 weight ratio) for anionic formulations and 0.5:5:1 (2.35:2.9:1 weight ratio) for cationic formulations, diluted to 0.01 mg/mL (DNA) in OptiMEM (Invitrogen, Paisley, UK) for *in vitro* transfections, diluted to 0.005 mg/mL (DNA) in sterile water for biophysical characterisation and diluted to 0.32 mg/mL (DNA) in sterile water for *in vivo* experiments. Six nanocomplex formulations were produced (Table 1), with a targeting peptide neurotensin (Nt), a scrambled neurotensin (NtS) and a non-targeting K_{16} peptide. Size and charge of liposomes, nanocomplexes and nanospheres was analysed using a Malvern Nano ZS (Malvern, UK) at a temperature of 25 °C, viscosity of 0.89 cP and a refractive index of 1.33.

2.4. In vitro transfections

The murine neuroblastoma cell line Neuro-2A (ATCC, Manassas, VA, USA) was maintained in Dulbecco's Modified Eagle Medium, 1% non-essential amino acids, 1 mM sodium pyruvate and 10% FCS (Invitrogen, Paisley, UK) at 37 °C in a humidified atmosphere in 5% carbon dioxide. Cell transfections were performed as previously described [25], briefly, cells were seeded at 2×10^4 per well in 96-well plates in 175 μL of complete. 24 h later 25 μL of the nanocomplex formulations (Table 1) in OptiMEM, containing 0.25 μg of plasmid DNA was added to the cells in replicates of six. Plates were centrifuged at 1500 rpm for 5 min (400× g) and incubated for 24 h at 37 °C. Cells were then lysed and a chemiluminescence assay performed to measure transfected luciferase activity (Promega, Southampton, UK) and protein concentration determined using a Bio-Rad protein assay (Hemel Hempstead, UK). Luciferase activity was expressed as RLU per milligram of protein. Cell viability assays were performed with the CellTiter 96 Aqueous One Solution Cell Proliferation Assay (Promega, Southampton, UK). Luciferase, protein concentration and toxicity measurements were performed in an Optima Fluostar microplate reader (BMG Labtech, Aylesbury, UK).

2.5. In vivo Brain delivery

All animal experiments were carried out with licences issued in accordance with the United Kingdom Animals (Scientific Procedures) Act 1986 (UK). For all experiments male Wistar rats (B&K Universal, Hull, UK) were anaesthetised and placed in a stereotactic frame, burr holes were drilled to allow cannula implantation to corpus callosum on the left and striatum on the right hand side of the brain was via a 220 μm outer diameter fused silica cannula at a rate of 0.5 μL/min at each site (2.5 μL for corpus callosum and 5 μL for striatum) using an infusion pump (World Precision Instruments, Inc, Sarasota, FL, USA). Following infusion, the

Table 1
LPD nanocomplex composition and associated size and zeta potential. Measurements were taken immediately after formation and 150 days post, as measured by dynamic light scattering.

LPD Nanocomplex	Charge Ratio (L:P:D)			Size (nm)		Zeta PD (mV)	
	Liposome	Peptide	DNA	Day 0	Day 150	Day 0	Day 150
Cat K_{16}	Anionic Liposome (0.5)	K_{16} (5)	pCI-Luc/eGFP (1)	196.5 (±4.4)	147.8 (±2.6)	+36.1 (±0.5)	+37.4 (±0.6)
Ani K_{16}	Anionic Liposome (3)	K_{16} (2)	pCI-Luc/eGFP (1)	170.6 (±7.1)	159.5 (±3.0)	−44.4 (±4.2)	−61.1 (±0.5)
Cat NtS	Anionic Liposome (0.5)	NtS (5)	pCI-Luc (1)	181.1 (±4.5)	153.2 (±2.9)	+31.5 (±0.7)	+31.3 (±2.2)
Ani NtS	Anionic Liposome (3)	NtS (2)	pCI-Luc (1)	254.0 (±3.3)	182.8 (±5.2)	−61.8 (±2.2)	−55.5 (±0.8)
Cat Nt	Anionic Liposome (0.5)	Nt (5)	pCI-Luc/eGFP (1)	216.9 (±6.8)	172.4 (±2.1)	+30.0 (±1.1)	+31.6 (±0.5)
Ani Nt	Anionic Liposome (3)	Nt (2)	pCI-Luc/eGFP (1)	177.6 (±1.4)	150.1 (±5.8)	−61.6 (±6.5)	−65.4 (±3.3)

cannula was left in situ for 5 min and withdrawn at a rate of 1 mm/min. Animals were killed by transcardial perfusion fixation using 4% paraformaldehyde (pH 7.4) under terminal anaesthesia. Animals were culled 48 h after administration with cationic and anionic nanospheres ($n = 2$ per nanosphere) and cationic and anionic liposomes ($n = 3$ per formulation, Supplementary Table 3) for analysis by fluorescence histology. Rats administered with cationic or anionic nanocomplexes containing targeting peptide Nt or the control peptide K_{16} (Table 1) ($n = 4$ per formulation and time point) were culled at 4 and 48 h after treatment for analysis by MRI and fluorescence histology.

2.6. MRI

MRI measurements were performed on a 9.4T VNMRS horizontal bore scanner (Varian Inc. Palo Alto, CA) using a 59/26 Rapid quadrature volume coil. Fixed rat brains were imaged using a T_1-weighted gradient echo 3D sequence (TR = 17 ms, TE = 4 ms, FA = 52°, 40 μm isotropic resolution, Ave = 6). Distribution volumes were measured by manually segmenting the hyperintensities caused by the gadolinium containing nanocomplexes using Amira (Visage Imaging Inc, San Diego, CA, USA).

2.7. Histological assessment

Brains were sectioned as 35 μm slices using a Leica CM1850 cryostat (Leica Microsystems, Wetzlar, Germany), washed with phosphate buffered saline and mounted in Vectashield (Vectorlabs, Burlingame, CA) on gelatin-coated slides and coverslipped, prior to fluorescent imaging with a Leica DM5500 microscope (Leica Microsystems, Wetzlar, Germany) and digital camera (MBF, Germany).

2.8. LA-ICP-MS

The laser ablation system (UP-266 Macro LA system, Nd:YAG λ 266 nm, New Wave Research, Cambridgeshire, UK) was configured to perform multiple parallel

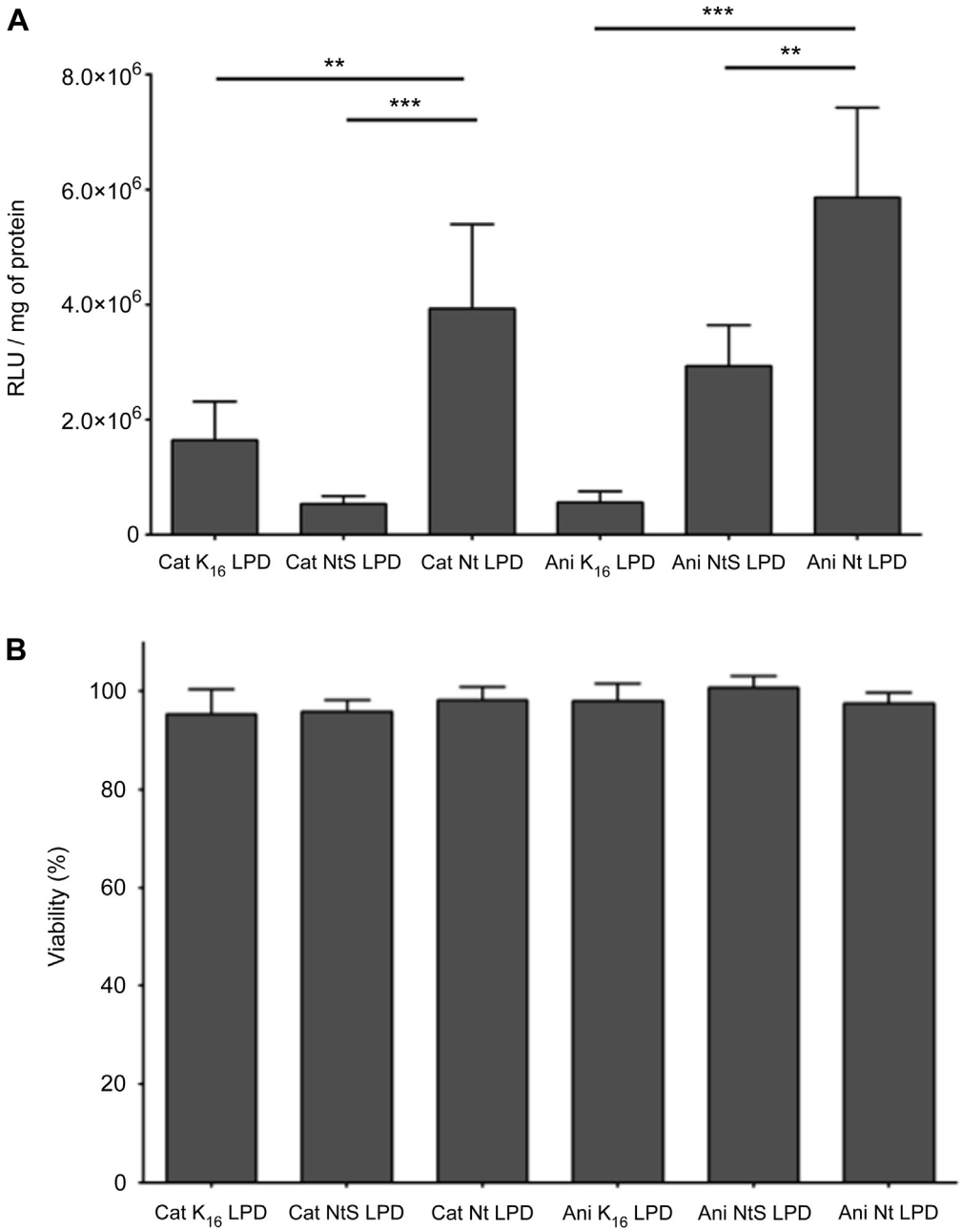

Fig. 1. *In vitro transfection and viability assays of cationic and anionic nanocomplexes in Neuro-2A cells*. Transfection efficiency and targeting specificity of the nanocomplexes as cationic and anionic formulations containing the targeted peptide Nt compared to two non-targeted formulations containing peptides, K_{16} and NtS measured by a luciferase activity assay (A). Cell viability after incubation with targeted compared to non-targeted as both cationic and anionic nanocomplex formulations (B). Values are the means of 6 replicates ± standard deviation with *t*-tests performed to calculate significant differences. $^{**}p < 0.01$, $^{***}p < 0.001$.

line rastering to generate elemental (2D) distribution maps. A laser beam diameter of 155 μm was utilised for interrogation of sections. Laser energy was in the range of 1.4 mJ at a frequency of 10 Hz, and the scanning speed was set to 60 μm/s. The interrogated area was in the region of 140 mm^2. The line rasters were separated by 310 μm, to prevent contamination of adjacent tissue with previous line raster runs. Complete analysis runtime was 178 min per section. Elemental maps were produced using the Graphis software package (Kylebank Software Ltd., Ayr, UK). The isotopes ^{157}Gd and ^{57}Fe were monitored in a time-resolved mode using an Agilent 4500 ICP-MS and were selected on the basis of high-percentage abundance and minimal interferences.

2.9. qRT-PCR

Rat brains ($n = 3$ per formulation) were collected in RNAlater (Invitrogen, Paisley, UK) and total RNA was extracted using the RNeasy kit according to the manufacturer's instructions (Qiagen, Crawley, UK). RNA was checked for integrity using the Agilent 2100 Bioanalyzer (Wokingham, UK) and all samples had a RNA integrity number (RIN) of more than 8 indicating high quality RNA. Prior to reverse transcription, each RNA sample underwent DNase treatment (Invitrogen) to eliminate any potential genomic DNA contaminants. First-strand DNA was synthesized from 1 μg of DNase-treated RNA, using random hexamers and Superscript II reverse transcriptase (Invitrogen, Paisley, UK) in a 1 h reaction at 37 °C eGFP, rat Succinate dehydrogenase complex subunit A (Sdha), rat Ribosomal protein L13 (Rpl13) and rat beta actin mRNA levels were then quantified by SYBR Green quantitative real-time polymerase chain reaction (qPCR) using an ABI PRISM 7000 Sequence Detection System (Applied Biosystems, Warrington, UK). The qPCR assay conditions were: stage 1, 50 °C for 2 min; stage 2, 95 °C for 10 min; stage 3, 95 °C for 15 s, then 60 °C for 1 min; repeated 40 times. Amplification efficiency was 102% (eGFP), 102% (beta actin), 103% (Rpl13), and 105% (Sdha). Copy numbers for eGFP and the three housekeeping genes were derived from standard curves constructed of purified PCR products generated for each specific primer pair ranging from 107 to 101 copies for eGFP, Rpl13, Sdha and beta actin. Copy numbers of iNOS were normalized against the geometric mean of Rpl13 and beta actin, which were the most stable genes.

2.10. Statistical analysis

Data presented in this study are expressed as the mean ± standard deviation and were analysed using a two-tailed, unpaired Student *t*-test where applicable.

3. Results

3.1. Biophysical characterisation of nanocomplexes

A series of targeted and non-targeted cationic and anionic nanocomplex formulations were generated and characterised for size and charge. Targeted anionic and cationic formulations both contained a peptide with a cationic oligolysine domain for efficient packaging of plasmid DNA and a neurotensin (Nt) receptor binding domain for cell targeting. The peptide was combined with an anionic liposome (DOPG:DOPE:DOPE-Rhodamine:GdDOTA(-$GAC_{12})_2$) and plasmid DNA which, at appropriate ratios and in the right order of mixing, created nanocomplexes with either a net cationic or anionic surface charge. The anionic liposome component of the nanocomplexes also contained lipids labelled with gadolinium and rhodamine to enable detection of nanocomplexes by both magnetic resonance imaging (MRI) and *ex vivo* histology [19,27–29] (Supplementary Table 1). In non-targeted formulations the Nt-targeting motif was scrambled (NtS) peptide or removed, leaving just K_{16}. The resulting nanocomplexes varied in size from 170 nm to 250 nm, while zeta potential measurements confirmed the predicted anionic and cationic surface charges of each formulation (Table 1). All of the liposomes and nanocomplexes formed had a polydispersity index of less than 0.3, indicating a monodisperse population of particles [30,31]. The properties of the nanocomplexes, based on their size and charge, were in the region stated by MacKay et al. required for increased delivery distribution when administered to the brain by CED [18].

3.2. In vitro cell transfections

In vitro cell transfections were performed on Neuro-2A neuroblastoma cells, to compare transfection efficiencies of anionic nanocomplexes with their cationic homologues. These cells were

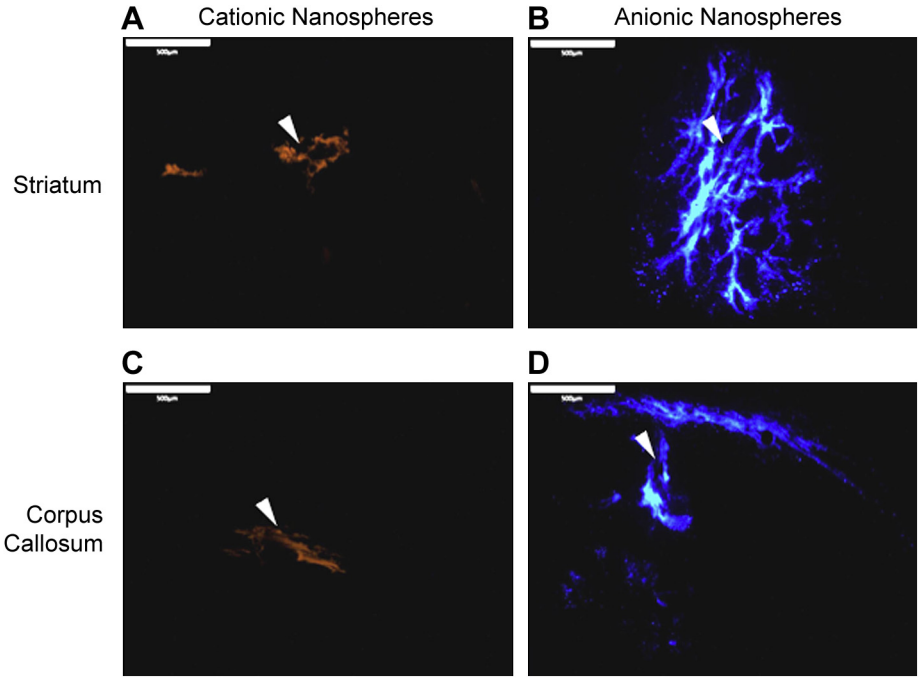

Fig. 2. *In vivo* distribution of cationic and anionic nanospheres in the striatum and corpus callosum after convection-enhanced delivery. Rats were administered with cationic (A,C) or anionic (B,D) fluorescently-labelled, 100 nm nanospheres into either the striatum (A,B) or corpus callosum (C,D). Tissue sections were analysed by fluorescence microscopy (A-D) to visualise the distribution of the nanospheres charge 48 h after administration from the injection site (white arrowheads). The anionic charged nanospheres were found to distribute further than their cationic counterparts. Scale bars = 500 μm.

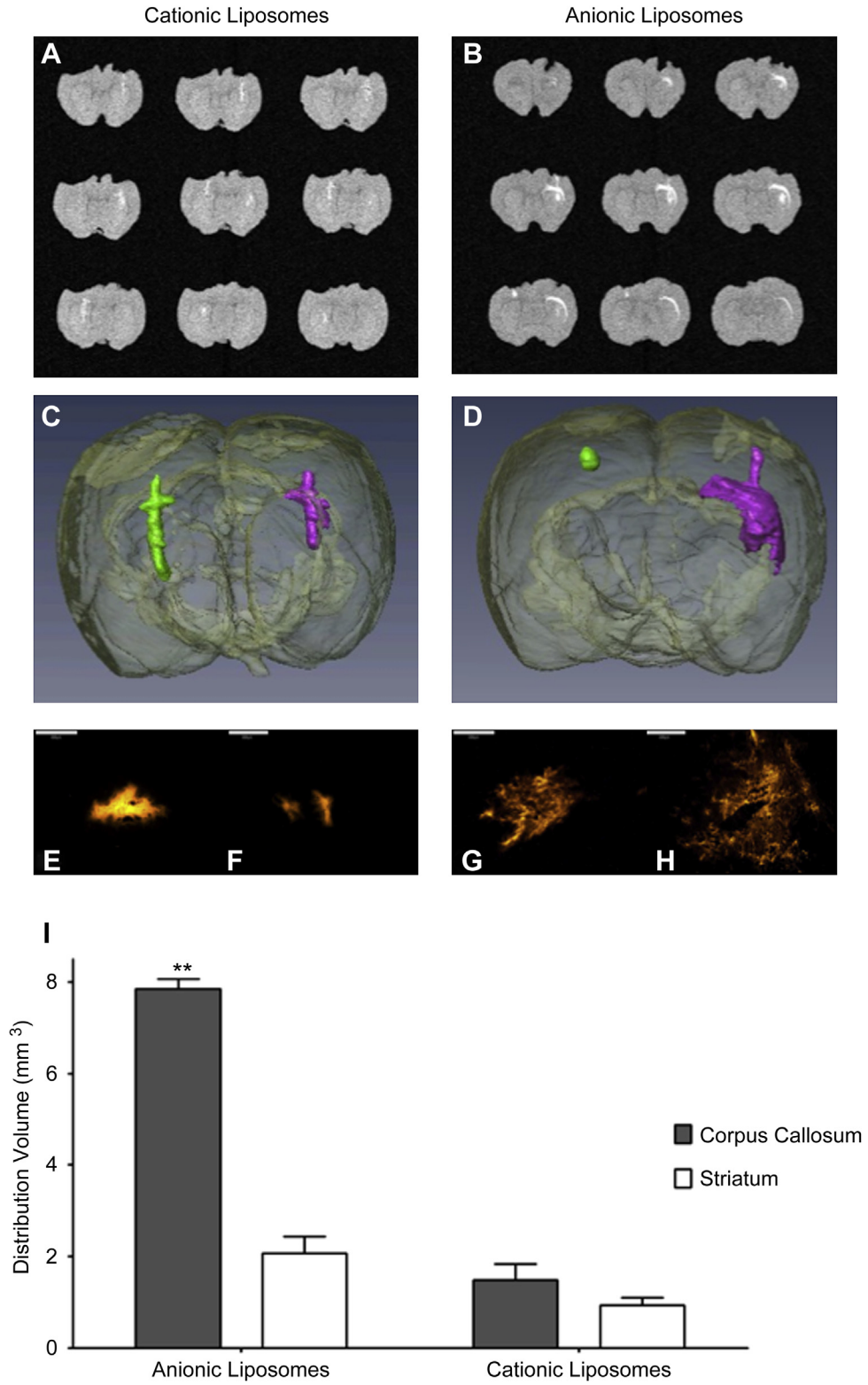

Fig. 3. MRI of gadolinium labelled cationic and anionic liposomes to measure *in vivo* distribution in the striatum and corpus callosum after convection-enhanced delivery. Optimised 3D T_1-weighted gradient echo scans were performed to allow visualisation of the gadolinium in the nanocomplexes, seen as hyperintensities, in both cationic (A) and anionic (B) liposomes. These data were reconstructed as 3D datasets to allow volumetric analyses between the cationic (C) and anionic (D) liposomes distribution after convection-enhanced delivery into the striatum (green) and corpus callosum (purple). Fluorescence microscopy was used to visualise cationic (E,F) and anionic (G,H) liposome distribution, by utilising the incorporated rhodamine label, in the striatum (E,G) and corpus callosum (F,H). The MRI data was used to calculate distribution of the cationic and anionic liposomes in the striatum and corpus callosum 48 h post administration (I). These results demonstrate that the anionic charged liposomes distribute further than the cationic equivalent liposomes. Values are the means of 3 replicates ± standard deviation with *t* tests performed to calculate significant differences. $^{**}p < 0.01$, scale bars = 500 μm.

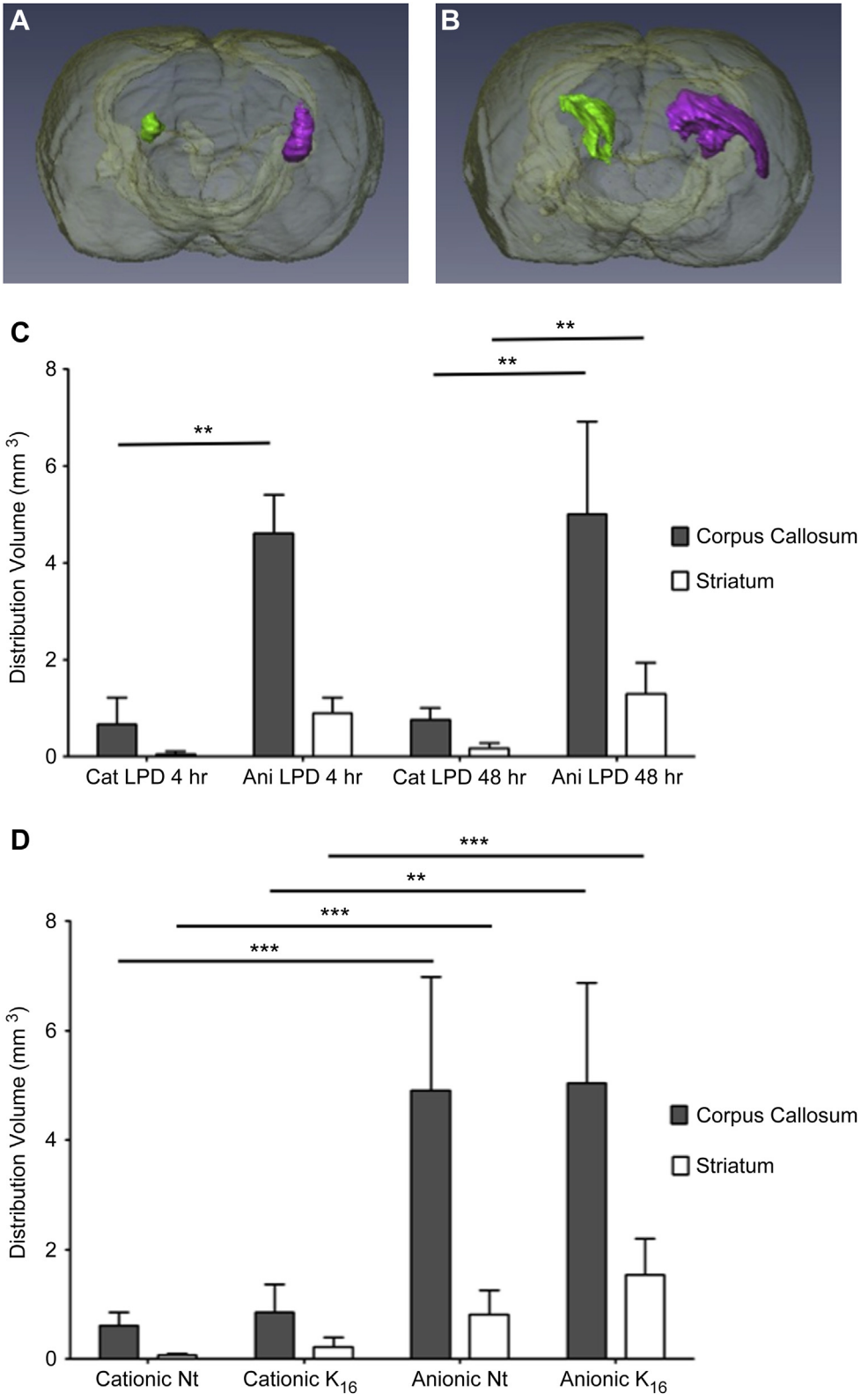

Fig. 4. *In vivo* distribution volume assessment of cationic and anionic nanocomplexes into the striatum and corpus callosum after convection-enhanced delivery. Reconstructed 3D datasets of optimised 3D T_1-weighted gradient echo scans allowed volumetric analyses between the cationic (A) and anionic (B) nanocomplexes distribution after convection-enhanced delivery. Distribution of the anionic and cationic nanocomplexes in the striatum (green) and corpus callosum (purple) at both 4 and 48 h post administration (C) and as Nt or K_{16} formulations was measured (D). Values are the means of 8 animals ± standard deviation with *t*-tests performed to calculate significant differences. $^{**}p < 0.01$, $^{***}p < 0.001$. (For interpretation of the references to colour in this figure legend, the reader is referred to the web version of this article.)

reported previously by us to be targeted by cationic nanocomplexes containing the Nt-targeted peptide [25]. Interestingly, the Nt receptor-targeted anionic formulations displayed similar levels of transfection efficiency to the cationic, Nt-targeted formulations. Both anionic and cationic Nt-targeting formulations displayed significant levels ($p < 0.01$) of transfection enhancement over both of their non-targeted nanocomplexes homologues containing either the NtS or K_{16} peptides (Fig. 1A), while cytotoxicity levels were minimal (Fig. 1B).

3.3. *In vivo* Brain delivery of nanospheres and liposomes

The hypothesis that anionic nanocomplexes would disperse further than cationic nanocomplexes in the brain by CED was tested

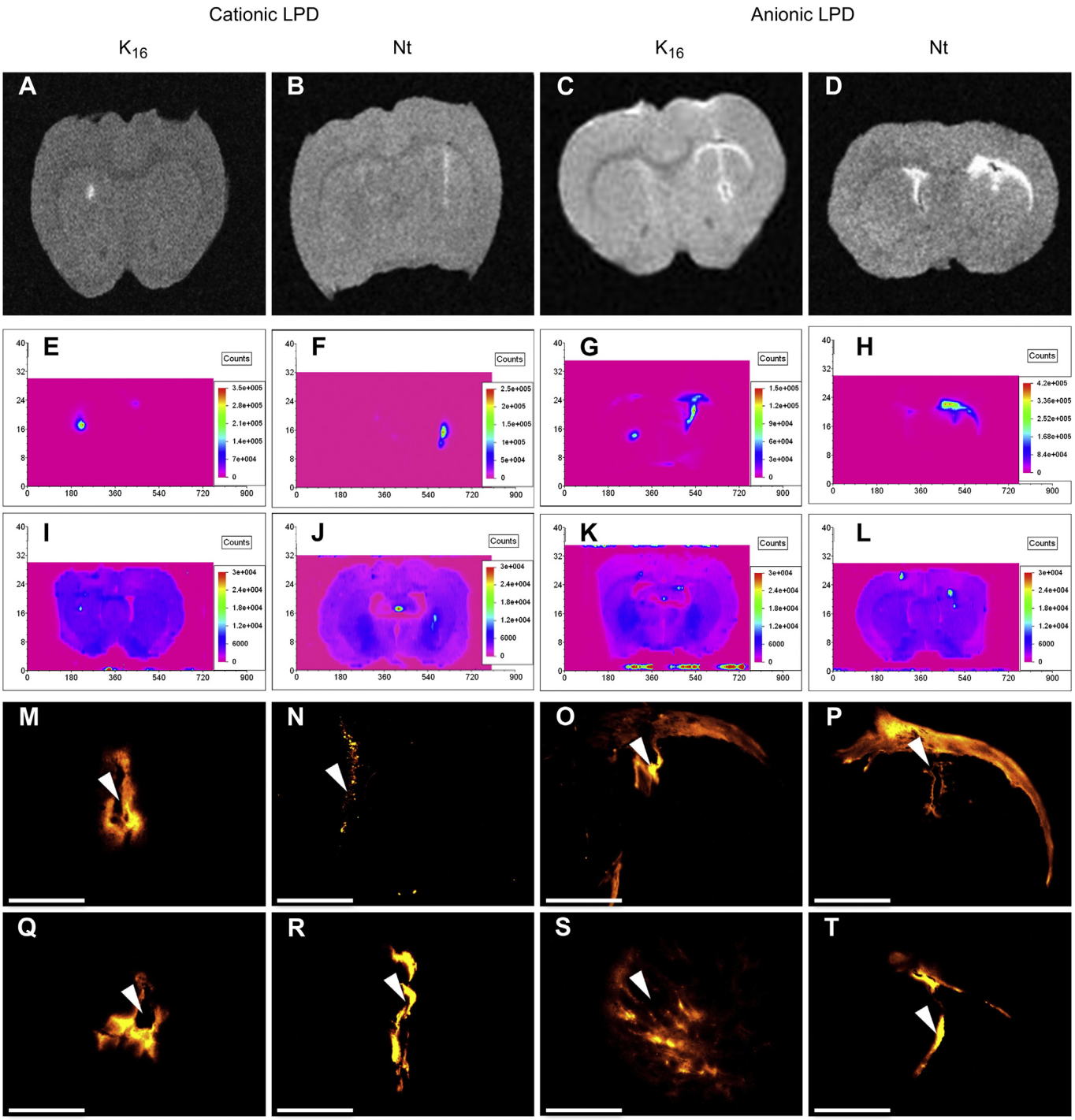

Fig. 5. Corroboration of MRI distribution of cationic and anionic Nt-nanocomplexes into the striatum and corpus callosum after convection-enhanced delivery. Optimised 3D T_1-weighted gradient echo scans were performed to allow visualisation of the gadolinium in the nanocomplexes, seen as hyperintensities, in cationic (A) and anionic (C) K_{16}-nanocomplex and cationic (B) and anionic (D) Nt-nanocomplexes. Corresponding LA-ICP-MS elemental maps of gadolinium (E-H) and iron (I-L) for cationic K_{16}-nanocomplexes (E,I), cationic Nt-nanocomplexes (F,J), anionic K_{16}-nanocomplexes (G,K) and anionic Nt-nanocomplexes (H,L) demonstrated MR signal intensities were due to gadolinium and not iron. Florescence microscopy was also utilised to confirm distribution of the cationic K_{16}-nanocomplexes (M,Q), cationic Nt-nanocomplexes (N,R), anionic K_{16}-nanocomplexes (O,S) and anionic Nt-nanocomplexes (P,T) by utilising the incorporated rhodamine lipid. White arrowheads = the injection sites. Scale bars = 500 μm.

with synthetic polystyrene nanospheres of 100 nm in size and cationic or anionic charges, both labelled with fluorophores ($n = 2$ per nanosphere). Nanospheres were administered by CED to rat brains in the striatum and corpus callosum then tissue sections were analysed by fluorescence microscopy at 4 h after administration (Fig. 2). In both regions of the brain the cationic nanospheres remained close to the cannula insertion site, while the anionic nanospheres showed a radius of dispersal of up to 2 mm from the site of the cannula tip, supporting the hypothesis that anionic particles would disperse better in the brain after CED. However, accurate analysis of dispersal of the nanospheres by fluorescence microscopy is difficult due to the nature of histology.

The hypothesis was then further tested by CED administration to rat brain of cationic and anionic liposomes of similar size, 163.1 nm and 140.8 nm respectively (Supplementary Table 3). The liposomes were labelled with gadolinium and rhodamine to allow the evaluation and quantification of distribution by MRI and fluorescence microscopy. It was apparent from both the MRI and fluorescence analysis that, as with the nanospheres, the cationic liposomes were restricted to the vicinity of the injection site while the anionic liposomes were more widely dispersed, with a radius of dispersal of up to 1 mm.

The raw data from the MRI analysis (Fig. 3A, B) was used to reconstruct a 3D image of the rat brain showing the extent of liposome distribution (Fig. 3C, D) and the distribution volumes for each liposome were then calculated in each area of the brain. The distribution volumes of anionic liposomes were four–fold higher in the corpus callosum than the cationic liposomes, while there was no significant difference between them in the striatum (Fig. 3I). These results were corroborated with fluorescence microscopy utilising the rhodamine incorporated into the liposome bilayer, which also displayed increased distribution in the anionic liposomes (Fig. 3E–H). The MRI also illustrated inaccuracy in the injection site and reflux of the nanocomplexes along the injection track (Fig. 3C, D). This increased distribution in the brain of anionic nanospheres and anionic liposomes was supportive evidence for further studies into the potential for widespread distribution of anionic nanocomplexes in the brain after CED.

3.4. In vivo Brain delivery of nanocomplexes

Neurotensin receptor-targeted and non-targeted, anionic and cationic nanocomplexes were prepared (Table 1) carrying the GFP reporter gene and administered to rat brains by CED in the striatum and corpus callosum. MRI analysis and 3D reconstructions indicated that the anionic nanocomplexes were more widely distributed than the cationics in both regions. Distribution volumes, calculated from the 3D reconstructions (Fig. 4A, B), were approximately seven-fold higher for anionic nanocomplexes in both the corpus callosum and striatum than cationic formulations (Fig. 4C, D). There were no significant differences in brain volume distribution at 48 h compared to 4 h by MRI (Fig. 4C), indicating that passive diffusion post-delivery was not occurring and no differences in distribution due to the peptide (Fig. 4D).

Analysis of the pattern of rhodamine distribution by fluorescence microscopy (Fig. 5M–T) and gadolinium by LA-ICP-MS (Fig. 5E–H) in brain sections indicated a similar distribution pattern of the MRI signal (Fig. 5A–D) for each sample. However, histological analysis of each brain sample revealed evidence of tissue damage and haemorrhage in almost all animals treated by CED due to the insertion of the cannula. We have shown previously that accumulation of iron from haemoglobin at sites of haemorrhage can lead to some ambiguity in MRI analysis [19,32]. To address this secondary analysis of tissue sections was performed by laser ablation inductively coupled mass spectrometry (LA-ICP-MS) to detect gadolinium distribution from the nanocomplex formulation and iron accumulation from haemorrhage. LA-ICP-MS analysis of ^{57}Fe in sections from brains treated with cationic and anionic nanocomplexes indicated a small degree of haemorrhage near the burr hole in the cranium and, additionally for the anionic sample, near to the site of injection in the corpus callosum (Fig. 5I–L). Two sections from the brain of each animal in each group were analysed for peak intensity of counts for ^{157}Gd and ^{57}Fe and correlated with peak signal intensity from MRI, which visually correlated with the ^{157}Gd signal distribution analysis (Table 2). Signals for ^{57}Fe were detected in each case with counts in the range of 3–9% of the ^{157}Gd counts. In samples where ^{57}Fe was relatively high compared to ^{157}Gd, anything above 35%, this was attributable to low counts for ^{157}Gd, of less than 15,000, due most likely to a poor injection, e.g., sample reflux, which was supported by the lack of MRI signal detected in the same samples. There was no significant reduction of Gd counts or MRI signal intensity from 4 h to 48 h.

3.5. Gene expression from nanocomplexes in the brain

Brain tissue sections analysed by fluorescence microscopy showed evidence of GFP expression (Fig. 6A–H), which appeared to correlate well with the MRI distribution analysis (Fig. 4A, B). GFP fluorescence was located in the vicinity of the cannula insertion site in the striatum for both cationic and anionic formulations. However, more widespread GFP expression was detected in the corpus callosum, particularly for the anionic formulations (Fig. 6B, D, F, H). As autofluorescence can be problematic with GFP fluorescence analysis, gene expression was also analysed by quantitative PCR amplification of mRNA (Fig. 6I) from the two regions of the brain. Highest expression levels were achieved by the cationic formulations in the corpus callosum, however the anionic formulations appeared to give comparable levels of expression to the other cationic formulations. The Nt targeting peptides gave higher levels of transfection than those containing the non-targeted K_{16} peptide in all cases, suggesting targeting with both anionic and cationic formulations.

4. Discussion

Systemic delivery of gene therapies to the brain is highly inefficient due to the impermeability of the blood brain barrier and so

Table 2
In vivo LPD nanocomplex LA-ICP-MS and MRI assessment. LA-ICP-MS was used to measure the peak intensity of iron (Fe) and gadolinium (Gd) in the brain samples on both left and right sides and then compared to the MRI peak signal intensity.

LPD Nanocomplex	Timepoint (h)	Fe counts		Gd counts		MRI peak intensity	
		L	R	L	R	L	R
Cat K_{16}	4	14700	11700	152000	15100	1.9023	1.0585
		15800	24500	84000	112000	1.9776	2.0587
	48	12800	2780	359000	42900	1.9636	1.0051
		3060	5650	1930	191000	1.0237	1.7054
Ani K_{16}	4	4230	4820	88700	153000	2.3509	2.2860
		10100	21600	182000	273000	2.0083	2.08
	48	13100	6910	575000	23200	1.8359	1.1648
		3640	14000	120000	404000	1.7121	1.8367
Cat Nt	4	13500	4700	247000	16300	1.3918	0.9266
		19200	5580	270000	6340	1.2937	1.1338
	48	1860	1100	1420	12400	0.9526	1.4698
		6750	36100	276000	5590	1.9917	1.0746
Ani Nt	4	19400	6360	415000	59200	2.8518	1.7748
		6410	4090	202000	104000	2.5513	1.9248
	48	7820	7030	65000	1720	2.1743	1.0820
		23500	4530	326000	7640	2.0763	1.0517

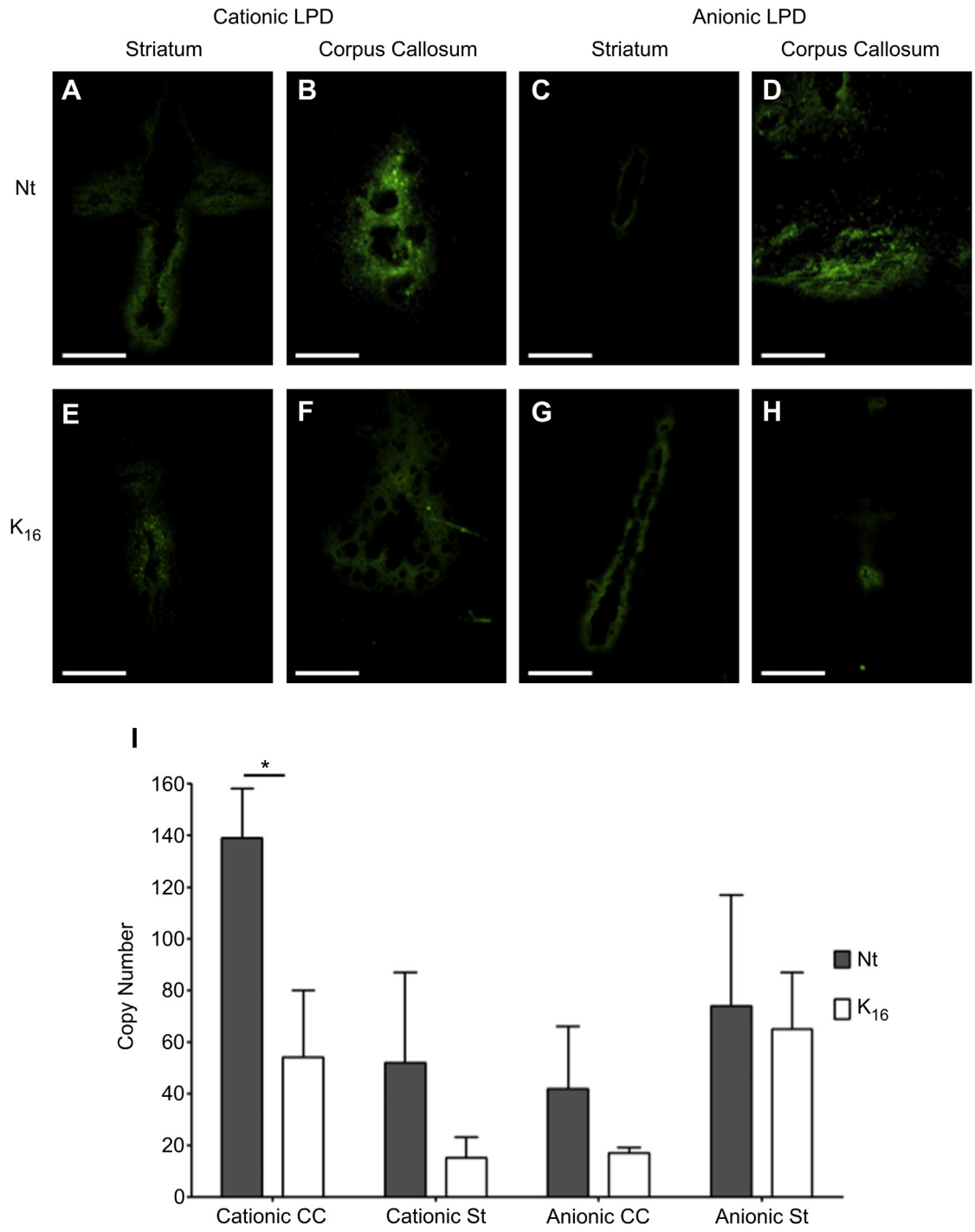

Fig. 6. Effective reporter gene delivery to the striatum and corpus callosum by cationic and anionic, with Nt targeting and K_{16} *non-targeting LPDs assessed by ex vivo fluorescence microscopy and qRT-PCR*. Fluorescence microscopy of the eGFP reporter gene was used to visualise cationic (A,B) and anionic (C,D) Nt-nanocomplex gene delivery in the striatum (A,C) and corpus callosum (B,D). eGFP expression mediated by cationic (E,F) and anionic (G,H) K_{16}-nanocomplex in the striatum (E,G) and corpus callosum (F,H) was also visualised. Functional delivery of the eGFP plasmid by the cationic and anionic nanocomplexes with Nt and K_{16} peptides was also assessed *ex vivo* with qRT-PCR (I). Values represent the mean of 3 animals per group ± standard deviation with *t*-tests performed to determine significant differences. $^{*}p < 0.05$, scale bars = 500 μm.

direct injection methods are under development. CED is the most effective method of direct injection, but anionic or neutral nanoparticles are required to achieve widespread dispersal [18]. Synthetic gene delivery formulations, however, are most often self-assembling formulations of cationic liposomes or cationic polymers that form strongly cationic nanocomplexes. While effective for DNA packaging and cell binding leading to strong transfection of some applications, their cationic charge is problematic *in vivo* in that it leads to non-specific interactions with negatively charged cellular and extracellular matrix components, serum proteins and enzymes. This can lead to aggregation and rapid clearance from the circulation by the reticuloendothelial system following systemic administration [33], hepatotoxicity [34] and a strong inflammatory response [35]. PEGylation sterically stabilizes cationic

nanoparticles, which minimizes their non-specific interaction *in vivo*, and thus may prolong the circulation time leading to nucleic acid accumulation in tissues other than liver, including tumours [36,37], but PEGylation may also impede cell uptake and endosomal escape yielding lower levels of gene expression [38]. We therefore decided to develop anionic, non-PEGylated nanocomplex formulations for brain delivery.

Nucleic acid packaging into anionic self-assembling complexes has been achieved by three general strategies; 1) combining anionic liposomes with polycationic protamine as an electrostatic bridge between the liposome and the nucleic acid [23,24], 2) combining anionic liposomes with calcium cations as the bridge [39–41], or, 3) forming an electrostatic coating of polyglutamate around a core cationic nanoparticle [42–44]. *In vivo* studies with all strategies have been reported [23,39,44,45] with evidence of efficacy and improved toxicity and safety compared to cationic formulations. Anionic liposomes injected systemically displayed much lower levels of liver accumulation than cationic liposomes [46] while anionic nanoparticles have been used to prolong circulation time and to increase delivery to tumours by passive targeting utilising the enhanced permeability and retention effect [43,45–47] in one case with a targeting moiety [23].

In seeking to develop new more efficient nanocomplexes for widespread dispersal of transfection in the brain by CED, we first examined the effect of charge on distribution of nanoparticles utilising both fluorescent nanospheres and fluorescent, gadolinium-labelled liposomes with cationic and anionic charges. Techniques of analysis included fluorescence microscopy analysis of both nanospheres and liposomes, and MRI in whole brains for the liposomes. In both settings the distribution of the anionic species was more widespread than the equivalent cationic species of similar size. Nanocomplex formulations of lipids and peptides labelled with fluorophore and gadolinium, also distributed further when their surface charge was anionic rather than cationic. Further analysis by LA-ICP-MS provided supportive evidence that the MRI in each case was unambiguously attributable to the distribution of gadolinium associated with the nanocomplex. This is important for *in vivo* work, and possibly for clinical studies, as MRI analysis of the gadolinium distribution alone is sufficient to determine the nanocomplex distribution, which can be measured in real time and at multiple time points. MRI allows accurate quantification of distribution, which is not possible by other techniques such as fluorescence microscopy analysis of tissue sections. In addition MRI illustrated the difficulty in accurately hitting the injection site of interest, as on occasion nanocomplex reflux up the needle track could be seen.

Anionic nanocomplex distribution volume in the striatum was significantly less than the same formulation in the corpus callosum, which is due, most likely, to the more compact nature of the striatum requiring pericellular transport, whilst in the corpus callosum the nanocomplexes were better able to travel between the nerve fibres. Thus, in the striatum, the size of the anionic liposomes, around 140 nm, may be a significant factor in limiting their distribution by CED. The distribution of the nanoparticles examined here is governed by convection rather than diffusion, as there was no increase in distribution detected 48 h after injection, which also indicates the potential for monitoring of delivery for several days after treatment. In future studies, it might be advantageous to formulate smaller nanocomplexes and to modify the coating to include a PEG layer to increase the distribution by diffusion as recently described by Nance et al. [20].

The qRT-PCR analysis demonstrated that the cationic nanocomplexes with the neurotensin targeting peptide had the greatest expression in the corpus callosum. In both cationic and anionic nanocomplexes the neurotensin peptide appeared to demonstrate higher transfection efficiencies when compared to the non-targeted control. However, due to variability and sample size only the neurotensin-targeted cationic nanocomplexes in the corpus callosum were statistically significant. Despite the anionic nanocomplexes not achieving the same expression *in vivo* as the cationic, the results offer promise that with minor modifications transfection efficiency can be significantly increased. This indicates that these anionic nanocomplexes, with their improved distribution, can be used to deliver therapeutic DNA to a larger volume than their cationic counterparts and still deliver the therapeutic payload to the appropriate cells.

The versatility of the nanocomplex platform described here allows for further optimisation by changing of the targeting moieties leading to specific cellular uptake of a defined cell type. Also, the liposome bilayer could be altered to include other imaging tracers or to further enhance the transfection efficiency or distribution properties. The promising results presented here suggest that these nanocomplexes could potentially used in the delivery of therapeutic genes to white matter diseases such as multiple sclerosis and Alzheimer's disease in humans as the delivery is greatest in the corpus callosum, affording large coverage. Therefore these results, taken alongside other clinical trials of CED [48–50], demonstrated that combining CED with anionic nanocomplexes has great potential for the treatment of a wide range of clinical neurodegenerative diseases.

5. Conclusions

In this study we have developed anionic nanocomplex formulations of liposomes, cationic-targeting peptides and plasmid DNA which we have shown to have increased distribution in the brain, particularly in the corpus callosum, by MRI, fluorescence histology and LA-ICP-MS. Neurotensin receptor-mediated transfection was demonstrated by GFP expression and qRT-PCR analysis, clearly showing that our nanocomplexes have real potential for the treatment of a wide range of neurodegenerative diseases.

Acknowledgements

This work was funded by the Engineering and Physical Sciences Research Council (EPSRC; EP/G061521/1). The British Heart Foundation funded ML for the MRI scanner. We would like to thank the Department of Biochemical Engineering, UCL for use of their Malvern Nano ZS and also Dr Mauro Botta from the Università del Piemonte Orientale "Amedeo Avogadro" for providing the gadolinium labelled lipid.

Appendix A. Supplementary data

Supplementary data related to this article can be found at http://dx.doi.org/10.1016/j.biomaterials.2013.07.081.

References

[1] Srikanth M, Kessler JA. Nanotechnology-novel therapeutics for CNS disorders. Nature Rev Neurol 2012;8:307–18.
[2] Davis ME, Chen Z, Shin DM. Nanoparticle therapeutics: an emerging treatment modality for cancer. Nat Rev Drug Discov 2008;7:771–82.
[3] Davis ME, Zuckerman JE, Choi CHJ, Seligson D, Tolcher A, Alabi CA, et al. Evidence of RNAi in humans from systemically administered siRNA via targeted nanoparticles. Nature 2010;464:1067–70.
[4] Ott MG, Schmidt M, Schwarzwaelder K, Stein S, Siler U, Koehl U, et al. Correction of X-linked chronic granulomatous disease by gene therapy, augmented by insertional activation of MDS1-EVI1, PRDM16 or SETBP1. Nat Med 2006;12:401–9.
[5] Orive G, Anitua E, Pedraz JL, Emerich DF. Biomaterials for promoting brain protection, repair and regeneration. Nat Rev Neurosci 2009;10:682–92.

[6] Gabizon AA, Shmeeda H, Zalipsky S. Pros and cons of the liposome platform in cancer drug targeting. J Liposome Res 2006;16:175–83.
[7] Kawakami S, Hashida M. Targeted delivery systems of small interfering RNA by systemic administration. Drug Metab Pharmacokinet 2007;22:142–51.
[8] Modi G, Pillay V, Choonara YE. Advances in the treatment of neurodegenerative disorders employing nanotechnology. Ann N Y Acad Sci 2010;1184:154–72.
[9] Fenske DB, Chonn A, Cullis PR. Liposomal nanomedicines: an emerging field. Toxicol Pathol 2008;36:21–9.
[10] Dadashzadeh S, Vali AM, Rezaie M. The effect of PEG coating on in vitro cytotoxicity and in vivo disposition of topotecan loaded liposomes in rats. Int J Pharm 2008;353:251–9.
[11] Bobo RH, Laske DW, Akbasak A, Morrison PF, Dedrick RL, Oldfield EH. Convection-enhanced delivery of macromolecules in the brain. Proc Natl Acad Sci U S A 1994;91:2076–80.
[12] White E, Bienemann A, Megraw L, Bunnun C, Gill S. Evaluation and optimization of the administration of a selectively replicating herpes simplex viral vector to the brain by convection-enhanced delivery. Cancer Gene Ther 2011;18:358–69.
[13] White E, Bienemann A, Sena-Esteves M, Taylor H, Bunnun C, Castrique E, et al. Evaluation and optimization of the administration of recombinant adeno-associated viral vectors (serotypes 2/1, 2/2, 2/rh8, 2/9, and 2/rh10) by convection-enhanced delivery to the striatum. Hum Gene Ther 2011;22:237–51.
[14] Chen MY, Hoffer A, Morrison PF, Hamilton JF, Hughes J, Schlageter KS, et al. Surface properties, more than size, limiting convective distribution of virus-sized particles and viruses in the central nervous system. J Neurosurg 2005;103:311–9.
[15] Gillies GT, Smith JH, Humphrey JAC, Broaddus WC. Positive pressure infusion of therapeutic agents into brain tissues: mathematical and experimental simulations. Technol Health Care 2005;13:235–43.
[16] Voges J, Weber F, Reszka R, Sturm V, Jacobs A, Heiss WD, et al. Clinical protocol. Liposomal gene therapy with the herpes simplex thymidine kinase gene/ganciclovir system for the treatment of glioblastoma multiforme. Hum Gene Ther 2002;13:675–85.
[17] Wakabayasi T, Natsume A, Hashizume Y, Fujii M, Mizuno M, Yoshida J. A phase I clinical trial of interferon-beta gene therapy for high-grade glioma: novel findings from gene expression profiling and autopsy. J Gene Med 2008;10:329–39.
[18] MacKay JA, Deen DF, Szoka Jr FC. Distribution in brain of liposomes after convection enhanced delivery; modulation by particle charge, particle diameter, and presence of steric coating. Brain Res 2005;1035:139–53.
[19] Writer MJ, Kyrtatos PG, Bienemann AS, Pugh JA, Lowe AS, Villegas-Llerena C, et al. Lipid peptide nanocomplexes for gene delivery and magnetic resonance imaging in the brain. J Control Release 2012;162:340–8.
[20] Nance EA, Woodworth GF, Sailor KA, Shih T-Y, Xu Q, Swaminathan G, et al. A dense poly(ethylene glycol) coating improves penetration of large polymeric nanoparticles within brain tissue. Sci Transl Med 2012;4:149ra119.
[21] Lakkaraju A, Dubinsky JM, Low WC, Rahman YE. Neurons are protected from excitotoxic death by p53 antisense oligonucleotides delivered in anionic liposomes. J Biol Chem 2001;276:32000–7.
[22] Zelphati O, Szoka Jr FC. Liposomes as a carrier for intracellular delivery of antisense oligonucleotides: a real or magic bullet? J Control Release 1996;41:99–119.
[23] Chen Y, Bathula SR, Li J, Huang L. Multifunctional nanoparticles delivering small interfering RNA and doxorubicin overcome drug resistance in cancer. J Biol Chem 2010;285:22639–50.
[24] Yuan H, Zhang W, Du Y-Z, Hu F-Q. Ternary nanoparticles of anionic lipid nanoparticles/protamine/DNA for gene delivery. Int J Pharm 2010;392:224–31.
[25] Kenny GD, Villegas-Llerena C, Tagalakis AD, Campbell F, Welser K, Botta M, et al. Multifunctional receptor-targeted nanocomplexes for magnetic resonance imaging and transfection of tumours. Biomaterials 2012;33:7241–50.
[26] Kielar F, Tei L, Terreno E, Botta M. Large relaxivity enhancement of paramagnetic lipid nanoparticles by restricting the local motions of the GdIII chelates. J Am Chem Soc 2010;132:7836–7.
[27] Kenny GD, Kamaly N, Kalber TL, Brody LP, Sahuri M, Shamsaei E, et al. Novel multifunctional nanoparticle mediates siRNA tumour delivery, visualisation and therapeutic tumour reduction in vivo. J Control Release 2011;149:111–6.
[28] Mulder WJ, Strijkers GJ, van Tilborg GA, Griffioen AW, Nicolay K. Lipid-based nanoparticles for contrast-enhanced MRI and molecular imaging. NMR Biomed 2006;19:142–64.
[29] Erdogan S, Medarova ZO, Roby A, Moore A, Torchilin VP. Enhanced tumor MR imaging with gadolinium-loaded polychelating polymer-containing tumor-targeted liposomes. J Magn Reson Imaging 2008;27:574–80.
[30] Kim J-Y, Kim J-K, Park J-S, Byun Y, Kim C-K. The use of PEGylated liposomes to prolong circulation lifetimes of tissue plasminogen activator. Biomaterials 2009;30:5751–6.
[31] Ma P, Dong X, Swadley CL, Gupte A, Leggas M, Ledebur HC, et al. Development of idarubicin and doxorubicin solid lipid nanoparticles to overcome Pgp-mediated multiple drug resistance in leukemia. J Biomed Nano 2009;5:151–61.
[32] Pugh JAT, Cox AG, McLeod CW, Bunch J, Writer MJ, Hart SL, et al. Elemental imaging of MRI contrast agents: benchmarking of LA-ICP-MS to MRI. Anal Bioanal Chem 2012;403:1641–9.
[33] Nomoto T, Matsumoto Y, Miyata K, Oba M, Fukushima S, Nishiyama N, et al. In situ quantitative monitoring of polyplexes and polyplex micelles in the blood circulation using intravital real-time confocal laser scanning microscopy. J Control Release 2011;151:104–9.
[34] Kedmi R, Ben-Arie N, Peer D. The systemic toxicity of positively charged lipid nanoparticles and the role of Toll-like receptor 4 in immune activation. Biomaterials 2010;31:6867–75.
[35] Ikebe M, Kitaura Y, Nakamura M, Tanaka H, Yamasaki A, Nagai S, et al. Lipopolysaccharide (LPS) increases the invasive ability of pancreatic cancer cells through the TLR4/MyD88 signaling pathway. J Surg Oncol 2009;100:725–31.
[36] Guo J, Cheng WP, Gu J, Ding C, Qu X, Yang Z, et al. Systemic delivery of therapeutic small interfering RNA using a pH-triggered amphiphilic poly-L-lysine nanocarrier to suppress prostate cancer growth in mice. Eur J Pharm Sci 2012;45:521–32.
[37] Sato A, Choi SW, Hirai M, Yamayoshi A, Moriyama R, Yamano T, et al. Polymer brush-stabilized polyplex for a siRNA carrier with long circulatory half-life. J Control Release 2007;122:209–16.
[38] Amoozgar Z, Yeo Y. Recent advances in stealth coating of nanoparticle drug delivery systems. Wiley Interdiscip Rev Nanomed Nanobiotechnol 2012;4:219–33.
[39] Li J, Yang Y, Huang L. Calcium phosphate nanoparticles with an asymmetric lipid bilayer coating for siRNA delivery to the tumor. J Control Release 2012;158:108–14.
[40] Kapoor M, Burgess DJ. Efficient and safe delivery of siRNA using anionic lipids: formulation optimization studies. Int J Pharm 2012;432:80–90.
[41] Patil S, Rhodes D, Burgess D. Anionic liposomal delivery system for DNA transfection. AAPS J 2004;6:13–22.
[42] Green JJ, Chiu E, Leshchiner ES, Shi J, Langer R, Anderson DG. Electrostatic ligand coatings of nanoparticles enable ligand-specific gene delivery to human primary cells. Nano Lett 2007;7:874–9.
[43] Harris TJ, Green JJ, Fung PW, Langer R, Anderson DG, Bhatia SN. Tissue-specific gene delivery via nanoparticle coating. Biomaterials 2010;31:998–1006.
[44] Schlegel A, Bigey P, Dhotel H, Scherman D, Escriou V. Reduced in vitro and in vivo toxicity of siRNA-lipoplexes with addition of polyglutamate. J Control Release 2013;165:1–8.
[45] Mignet N, Richard C, Seguin J, Largeau C, Bessodes M, Scherman D. Anionic pH-sensitive pegylated lipoplexes to deliver DNA to tumors. Int J Pharm 2008;361:194–201.
[46] Lee S, Lee S-Y, Park S, Ryu JH, Na JH, Koo H, et al. In vivo NIRF imaging of tumor targetability of nanosized liposomes in tumor-bearing mice. Macromol Biosci 2012;12:849–56.
[47] Maeda H, Wu J, Sawa T, Matsumura Y, Hori K. Tumor vascular permeability and the EPR effect in macromolecular therapeutics: a review. J Control Release 2000;65:271–84.
[48] Gill SS, Patel NK, Hotton GR, O'Sullivan K, McCarter R, Bunnage M, et al. Direct brain infusion of glial cell line-derived neurotrophic factor in Parkinson disease. Nat Med 2003;9:589–95.
[49] Bruce JN, Fine RL, Canoll P, Yun J, Kennedy BC, Rosenfeld SS, et al. Regression of recurrent malignant gliomas with convection-enhanced delivery of Topotecan. Neurosurgery 2011;69:1272–80.
[50] Vogelbaum MA, Sampson JH, Kunwar S, Chang SM, Shaffrey M, Asher AL, et al. Convection-enhanced delivery of cintredekin besudotox (interleukin-13-PE38QQR) followed by radiation therapy with and without temozolomide in newly diagnosed malignant gliomas: phase 1 study of final safety results. Neurosurgery 2007;61:1031–8.